PHASE PLANE TRAJECTORIES OF THE MUSCLE SPIKE POTENTIAL

HOWARD JENERICK
From the Department of Physiology, Emory University, Atlanta

ABSTRACT To facilitate a study of the transmembrane action current, the striated muscle spike potential was recorded against its first time derivative. The specialized recording methods are described, as well as several mathematical transformations between a coordinate system in V, t, and the present coordinate system in V, dV/dt. The particular properties of the present recording method permitted an estimation for the "sodium" potential in muscle fibers at +39 mv. The maximum membrane conductance during spike production is in the order of 150 to 200 mmhos/cm^2. The changes in the shape of the recorded response indicate that the ionic currents and membrane conductances are reduced by Tris buffer or hypertonic Ringer's fluid. However, no marked changes in the properties of active membrane were observed when chloride ion was replaced by sulfate.

INTRODUCTION

Physiological responses do not occur instantaneously, but are generated by time-dependent processes. Accordingly, it is standard practice to record such responses as functions of time. This procedure illustrates qualitative aspects of the time dependence and permits the direct measurement of various response characteristics such as time constant, duration, frequency, etc. However, certain practical problems are encountered if a more detailed analysis of the shape of nerve and muscle action potentials is desired. Their complexity makes it difficult to obtain a rigorous description of their time course by selection and fitting of various types of equations to the records (*e.g.*, for nerve, see Rosenblueth, *et al.*, 1948). Replotting of the response on special graph paper is needed to test for exponential or power functions, while the extraction of first and second time derivatives by graphical methods is subject to error.

An alternate recording technique which reduces some of these difficulties is described here. This involves recording the spike potential V, in the phase plane, in which V is displayed against its first time derivative dV/dt. Because the slope of the response appears in these records, a more sensitive index of the response shape is obtained. In addition, the records are expanded at all inflection points, where $|dV/dt|$

reaches maximum values. It will be recalled that these regions in the conventional record in V, t, are compressed or steep and are therefore most difficult to analyze critically. Other useful features and the results of phase plane recording are presented below.

METHOD

Transmembrane spike potentials from sartorius muscle fibers of *Rana pipiens* were obtained by means of an impaling glass microelectrode and a neutralized input capacity preamplifier. The spike potential (V) was displayed *via* the horizontal amplifier of a dual beam oscilloscope. This signal was also led to an electronic differentiator as shown in Appendix Fig. 1. The differentiator generated a signal (proportional to dV/dt) which was displayed simultaneously *via* the channel A vertical amplifier. A time base sawtooth voltage was applied to the channel B vertical amplifier. The dual beam oscilloscope consequently permitted the display of the spike potential in the phase plane on channel A (V against dV/dt) and in the conventional coordinate system on channel B (V against t). (See the Appendix for further details.)

Stimuli were applied with a small bipolar metal electrode placed 5 to 10 mm from the recording site. The standard Ringer's fluid contained 110 mM NaCl, 2.5 mM KCl, 2.0 mM $CaCl_2$ and 2 mM phosphate buffer at pH 7.2 — 7.4. Laboratory temperatures ranged between 20° and 25°C.

RESULTS

Sine and Exponential Trajectories. Since the phase plane recording modifies the customary aspect of the muscle spike potential, it is useful for orientation to consider first the trajectories of several well known functions. The sine function illustrated in Fig. 1 is described by, $V/V_{max} = \sin \omega t$, where $\omega = 2\pi x$ frequency. Dif-

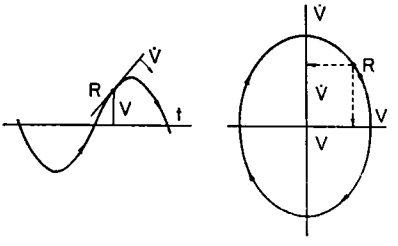

FIGURE 1 A sine wave illustrated in conventional coordinates (V, t) and in the phase plane (V, $\dot{V}$). At the point R, the signal has risen to voltage V and at this instant has a slope of dV/dt or $\dot{V}$. It can be seen that for a short time V will continue to increase and $\dot{V}$ decrease. The trajectory therefore, is developed clockwise in time as shown by the arrows.

ferentiating with respect to time; $(dV/dt)/\omega V_{max} = \cos \omega t$. Squaring and adding eliminates t, and gives $(V/V_{max})^2 + (dV/dt)^2/(\omega V_{max})^2 = 1$, the equation of an ellipse in the phase plane as shown in Fig. 1. The horizontal and vertical diameters are equal to $2V_{max}$ and $2\omega V_{max}$, respectively. This particular feature makes the sine

wave a convenient calibration signal (see Appendix). A frequently encountered function in biological recordings is an exponential of the following general type,

$$V - V_o = A \exp(kt), \tag{1.1}$$

where V_o is a reference voltage, A is a scale constant and k is a rate constant. It follows that

$$dV/dt = k \cdot A \exp(kt). \tag{1.2}$$

By eliminating t, the equation of a straight line is obtained

$$dV/dt = k(V - V_o). \tag{1.3}$$

Thus, all processes which are exponential in time will appear as linear trajectories, whose slopes are equal to the rate constants as may be seen by inspection of (1.1) and (1.3). Furthermore, equation (1.3) indicates that the extrapolation of any linear trajectory will intersect the V axis at the reference voltage (V_o) for the exponential process.

Spike Potential Trajectory. A spike potential somewhat resembles one period of the sine function and by analogy with Fig. 1, an elliptical trajectory is expected. However, Fig. 2 demonstrates that the peculiarities of the spike shape have modified the ellipse in several important details. Since the advancing foot of the spike rises exponentially in time (Tasaki and Hagiwara, 1957; Jenerick, 1957), the initial trajectory becomes linear with a slope, k_r (Fig. 2, portion *a*.)

A number of selected parameters which represent major features of the response are also indicated in the figure. V_r and V_s are the resting potential and spike potential, respectively. V_n is the negative after-potential, V_i is the first inflection point of the spike, and V^* is the firing point. $\dot{V}+$ and $\dot{V}-$ are the maximum rates of rise and fall. An approximately exponential process of slope k_f is also seen in this record. This region (*c*) lies below the second inflection point and leads toward the initiation of the negative after-potential, although this particular record shows more curvature in *c* than is usually observed.

Overshoot and Conductance. The trajectory shape in region *b* is currently under study since this portion is generated during the period of massive inward transmembrane ion flow (Jenerick, 1961). In many records, a significant portion of this region is approximately linear, as in Fig. 2. Extrapolation to the V axis indicates an "overshoot" potential that falls within the range expected for the sodium potential V_{Na} (Table I), although the slight curvature in *b* makes this determination somewhat arbitrary. When fitted into the Nernst equation, the overshoot potential predicts an internal Na^+ concentration of 24 mM, in agreement with published data. The presence of this linearity in the trajectory is consistent with the assumptions that (1) the sodium conductance (g_{Na}) reaches and briefly maintains a constant value soon after the first inflection point, while (2) the potassium conductance

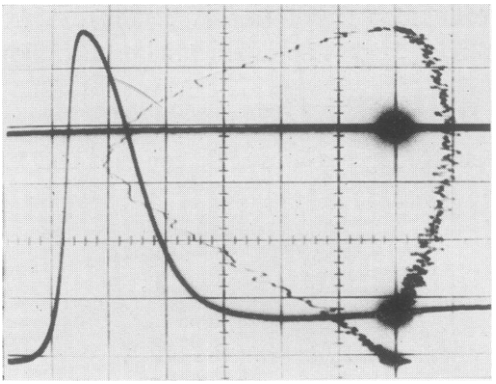

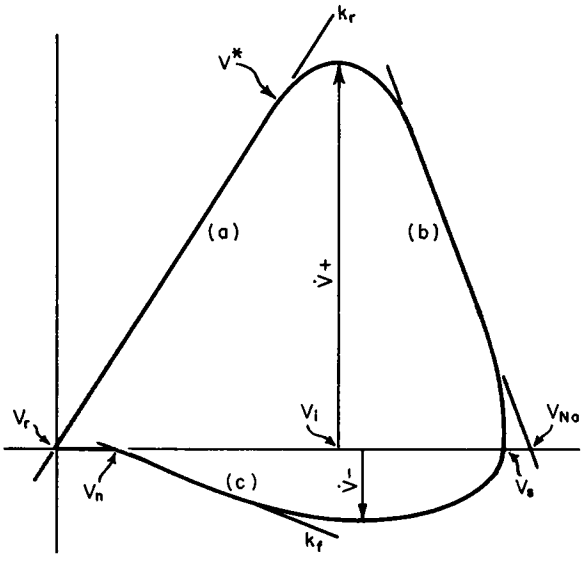

FIGURE 2(*upper*) Simultaneous record of a 112 mv muscle spike potential in (V, t) and $(V, \dot{V})$. The V axis (vertical) is common to both records as explained in the Appendix. Each vertical graticule mark spans 20 mv; each horizontal graticule mark spans ½ msec. or 100 v/sec. Note the accentuation of high frequency noise in $V, \dot{V}$.
FIGURE 2(*lower*) A smoothed tracing of the phase trajectory from the record above which depicts the constants which have been chosen to describe the response. Membrane excitation occurs at the approximate point indicated by the arrow V^*.

(g_K) remains at a negligible level. Thus, if g_K is small, the cable equation for a propagating action potential is reduced to

$$\frac{g_{Na}(V - V_{Na})}{C} = (d^2V/dt^2)/(k_r) - dV/dt \qquad (2.1)$$

where C is membrane capacitance (Jenerick, 1961). Since it is tentatively assumed

TABLE I

ESTIMATES OF V_{Na} AND g_{Na} FROM PHASE TRAJECTORIES

Exp. No.	V_{Na}	g_{Na}*	No.
	mv	*mhos/cm²*	
C-78	36	0.18	4
C-87	35	0.11	7
C-91	42	0.14	8
C-92	39	0.13	11
C-93	45	0.15	5
D-16-1	35	0.18	9
D-16-2	40	0.17	14
Group average	39 mv	0.15	(58)

* Based on calculations assuming a membrane capacitance of 6 μf/cm².

that g_{Na} is constant, 2.1 may be immediately integrated to yield a solution of the form,

$$V - V_{Na} = A \exp(-kt). \tag{2.2}$$

Equation (2.2) predicts a linear trajectory in the phase plane with a slope of $-k$ and an intercept of V_{Na}. Since portions of actual trajectories demonstrate or closely approximate this behavior, discrete values for g_{Na} may now be computed. Substituting 2.2 and its derivatives into 2.1, one obtains,

$$g_{Na} = C\frac{k}{k_r}(k + k_r)$$

Calculations for g_{Na} from 58 separate responses are listed in Table I. Unfortunately, this particular feature of the recording cannot be fully exploited, since the pre-peak linearity does not appear consistently in all experiments.

Slope Parameters. The averaged values for the selected parameters of spike trajectories from muscle fibers bathed in standard Ringer's fluid are listed in Table II under "phosphate buffer." The data are arranged to demonstrate the apparent interdependence of V_s and the constants. The data from Experiment C-98 illustrate the variations observed between the right and left sartorius muscles of one frog. These differences probably reflect normal biological variations or measurement errors and have no physiological significance, since the left-right difference bears no relation to the duration of exposure to Ringer's fluid (up to 2 hours), to the particular muscle chosen, or to possible dissection damage (the right muscle is customarily more difficult to isolate).

The usefulness of the selected parameters as predictors of membrane properties is under continuing study. It has already been reported that the initial rate constant k_r is equal to the factor $(2\ RC\theta^2)/a$ in the cable equation (Jenerick, 1957). (This

TABLE II

Exp. No.	V_a	$\dot{V}+$	$\dot{V}-$	k_r	k_f	V_n	V_i	No.	Buffer*
	mv	*v/sec.*	*v/sec.*	*msec.*$^{-1}$	*msec.*$^{-1}$	*mv*	*mv*		
C-117	129	580	160	9.1	3.4	26	77	7	Phosphate
C-98 R	126	500	130	—	—	15	78	6	"
C-98 L	124	550	150	—	—	17	77	7	"
C-88	124	525	145	9.3	2.8	20	75	7	"
C-96	121	470	140	8.2	3.2	19	71	6	"
C-115	115	440	120	7.7	2.7	19	69	9	"
M-45	113	450	107	—	—	—	—	5	"
C-96	112	450	125	9.1	2.8	18	61	6	"
Group average	121	495	135	8.7	3.0	22	73	(53)	
S-35	128	400	94	6.0	2.0	22	77	17	Tris‡
S-19	126	360	100	8.2	2.5	12	77	8	"
S-36	124	320	80	5.7	1.6	—	73	12	"
M-48	116	360	125	—	—	—	—	6	"
S-20	115	390	96	6.7	2.8	28	68	11	"
S-21	112	350	90	7.4	2.0	28	62	10	"
Group average	117	363	98	6.9	2.2	22	72	(64)	

* Buffers were used at a concentration at 1 to 3 mM at pH 7.1-7.4 in standard Ringer's fluid.
‡ tris (hydroxymethyl)aminomethane.

permitted equation 2.1 to be written as shown). In addition, the following relationships have been consistently observed (assuming the membrane capacitance remains constant during the response). The maximum inward and outward ionic currents of the spike potential are related to $\dot{V}+$ and $\dot{V}-$, respectively, while the membrane conductance during the terminal portion of the spike (region *c*, Fig. 2) is directly proportional to the rate constant k_f. V_i has not been correlated with any identifiable process in spike production, and our analyses indicate the membrane does not become active at this point as has been occasionally assumed. Instead, the membrane appears to fire about 30 μsec. earlier at the point where the initial trajectory departs from linearity. This firing potential V^* is indicated in Fig. 2 by a small arrow.

As expected, all parameters are influenced by the ionic composition of the Ringer's fluid. The effect of increased Ca^{++} ion concentration has been described previously (Jenerick, 1957). If the phosphate buffer is replaced by tris-(hydroxymethyl)aminomethane buffer, all parameters except the negative after-potential are decreased by 20 to 50 per cent, (Table II). The reason for this shift is unknown.

Experiments were also performed in which the spike magnitudes were deliberately altered by bathing muscles in a phosphate-buffered Ringer's with varied KCl concentration (1 to 5 mM). Averaged results from 150 fibers in 20 experiments are plotted in Fig. 3. During the summer months, some difficulty was experienced in

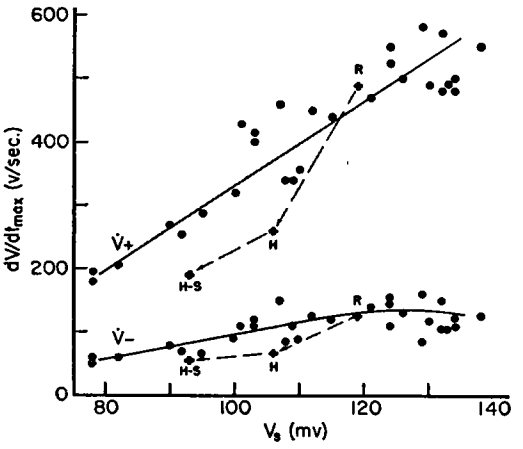

FIGURE 3(*a*) The maximum rates of rise ($\dot{V}+$) and fall ($\dot{V}-$) of the spike potential plotted against its magnitude (V_s). Each filled circle represents the average of measurements on 10 to 20 fibers. The crosses plot data from Table III (see text). Although actual values for $\dot{V}-$ are negative, the data is plotted above the origin for convenience.

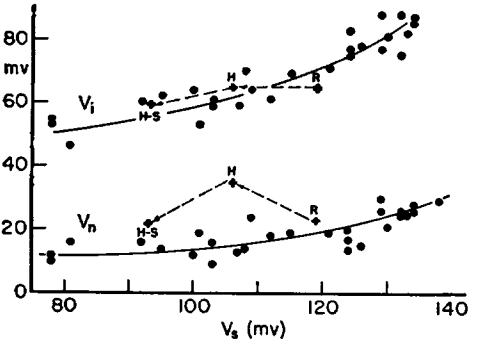

FIGURE 3(*b*) The potential at the first inflection point (V_i) and the initial value of the negative after-potential (V_n) plotted against the spike potential. Potentials are measured from the initial resting potential.

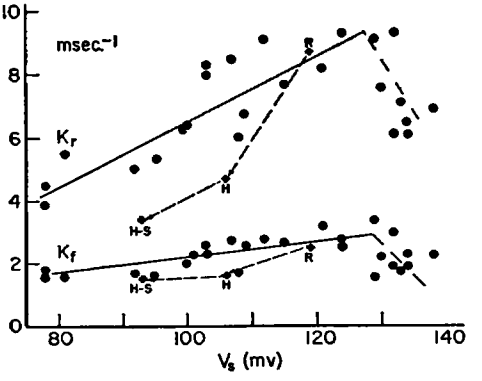

FIGURE 3(*c*) This figure presents the rate constants for the exponential foot of the spike potential (k_r) and for an exponential portion on the trailing edge of the spike (k_f). These processes are identified in Text Fig. 2. Both constants are seen to sag off at high values of V_s.

the form of lowered resting and spike potentials in the standard fluid. The data were observed to vary in direct proportion to alterations of the recorded spike height and it seems clear they are not primarily dependent on KCl concentration.

Chloride Replacement. To assess the possible role of the principal anion in the production of the spike potential, a sulfate-Ringer was substituted for the standard fluid. In order to abolish mechanical movements which follow depolarization caused by Cl^- withdrawal, the muscle was bathed initially in a hypertonic fluid before sulfate-Ringer was placed in the muscle chamber. The results of each fluid replacement are listed in Table III, and the group averages are plotted as

TABLE III

EFFECTS OF HYPERTONICITY AND Cl WITHDRAWAL

Exp. No.	V_s	$\dot{V}+$	$\dot{V}-$	k_r	k_f	V_n	V_i	No.	Fluid
	mv	*v/sec.*	*v/sec.*	*msec.*$^{-1}$	*msec.*$^{-1}$	*mv*	*mv*		*mM*
C-66	115	470	111	8.8	2.4	17	56	9	102 Na, 2 K, 1 Ca,
C-67	116	470	126	8.5	2.0	19	59	11	1.5 PO_4, 106 Cl
C-68	116	525	135	9.8	2.8	22	65	10	
C-69	120	515	122	8.2	2.5	23	70	6	
C-70	127	500	119	7.6	2.4	30	77	6	
C-71	120	470	145	9.4	2.8	24	61	7	
Group average	119	490	126	8.7	2.5	23	65	(49)	
C-68	106	290	73	5.3	1.8	33	66	14	Same as above +
C-70	103	210	53	3.9	1.3	38	64	8	300 sucrose
C-71	109	270	75	4.9	1.6	34	65	21	
Group average	106	260	67	4.7	1.6	35	65	(43)	
C-66	99	220	62	3.3	1.4	19	62	5	102 Na, 2 K, 8 Ca
C-68	94	180	61	3.3	1.8	27	59	3	1.5 PO_4, 60 SO_4,
C-70	85	160	51	3.6	1.3	20	57	6	345 sucrose
Group average	93	190	58	3.4	1.5	22	60	(14)	

crosses in Fig. 3. (Note that calcium chloride was increased to 8mM to account for the reduction of ionized calcium concentration by calcium sulphate formation.) Hypertonicity caused the greatest proportional reduction in most parameters. Thereafter, the replacement of the Cl^- ion by sulfate further lowered the resting and spike potentials, but this was expected. However, the withdrawal of Cl^- ion did not seem to modify the usual interdependence between the data and the spike potential, as indicated by the slopes in Fig. 3.

This evidence would suggest that the chloride ion does not carry a major fraction of the membrane current associated with the spike potential, and is in marked contrast to its effect on the resting potential and the after-potential.

DISCUSSION

There exist many second-order differential equations which cannot be solved and which are even difficult to interpret by inspection. Some of these govern the behavior of important non-linear physical devices (*e.g.*, feedback control systems, pendulums, oscillators) and various methods have been developed by which the system's performance may be visualized and understood. One approach involves the construction of a phase plane plot and an analysis of the trajectory by means of specialized techniques (Minorsky, 1947, Graham and McRuer, 1961). The action potential is similarly generated by various non-linear processes, and by analogy, it seemed likely that a phase plane trajectory of the spike, would lend itself more readily than a V, t record, to a quantitative analysis of the membrane response.[1] It had already been shown by Schmitt (1955) for example, how the V, dV/dt record might be used to calculate the energy release in the cell membrane during impulse propagation. Another previous application is that of Cole, *et al.* (1955) where phase plane trajectories were used to portray the results of machine computations of axon prepotentials and action potentials from the Hodgkin-Huxley equations.

The studies reported here were primarily concerned with the measurement of normal values and ranges for various selected features of the spike potential trajectory (Table II). In addition, an immediate result of the present recording system was the identification of a means for determining the peak membrane conductance and the equilibrium potential (V_{Na}?) for the overshoot (Table I). These data were obtained from the slope of a quasilinear region of the trajectory and lend support to the initial supposition that various important membrane properties are represented in the shape of the phase plane trajectory.

In the past, we had occasionally replaced phosphate by Tris buffer in Ringer's fluid and monitored the effects by the shape and magnitude of the spike potential in (V, t). No consistent effects were observed outside of a slight broadening of the spike, until the present techniques were developed. The results listed in Table II demonstrate that Tris buffer is not innocuous, and are all the more startling in view of the negligible effects previously observed.

Measurements were also made on the effects of replacing chloride by sulfate ion. The fiber twitching caused by spontaneous firing was controlled by the addition of 0.3 M sucrose to the Ringer's fluid. However, the effects of hypertonicity alone were greater than those associated with the absence of the chloride ion (Table III). The observed shift in the parameters indicates that one primary effect of a hypertonic Ringer's fluid is a large decrease in the spike height and in the maximum outward and inward ionic currents.

A previous attempt "to obtain a rigorous description of the time course of the

[1] The recording system employed here is regarded as a phase plane for purposes of presenting the observed relationships between V and dV/dt of the spike, although the actual trajectories do not have all the properties identified with a *mathematically* defined phase plane.

spike potential" was based on a graphical analysis of the shape of the V, t record of *axon* responses (Rosenblueth, *et al.*, 1948). As in the muscle fiber response (regions *a* and *c*, Fig. 2), exponential processes were found at the beginning and at the end of the axon spike potential. The associated rate constants of the axon spike at 25°C were reported as 21 msec.$^{-1}$ and 3.9 msec.$^{-1}$, respectively, in contrast to the averages for muscle obtained here of $k_r = 8.7$ msec.$^{-1}$ and $k_f = 3.0$ msec.$^{-1}$.

The rate constant k_r for the leading foot of the muscle spike is equal to $2\ RC\theta^2/a$ where R is myoplasm resistivity, C is membrane capacitance, θ is conduction velocity, and a is fiber radius. However, substitution of the relevant cell constants for nerve fibers do not agree with the 21 msec.$^{-1}$ value for the initial rate constant of the axon spike potential obtained by Rosenblueth, *et al.* This suggests that the cable equation (from which k_r is derived) cannot be applied directly to impulse conduction in the myelinated nerve fiber. In view of the participation of the nodes in impulse propagation and the unknown shunting effect of the internodes, this lack of agreement is not surprising.

It can be shown that the rate constant k_f in muscle is directly proportional to the membrane conductance during the terminal portion of the spike. However, it is not possible to do this for the myelinated axon response, and no further comment can be made on the value of 3.9 msec.$^{-1}$ (the final rate constant) reported by Rosenblueth, *et al.*

The other constants reported by Rosenblueth, *et al.* cannot be compared to those given in Table II, since they were obtained by an entirely different analytical approach, although an additional point requires comment. Their Fig. 4, apparently demonstrates a corner in $\dot{V}$ against t at each inflection point of the spike. This requires that the second time derivative of the spike $\ddot{V}$, which is proportional to the total membrane current density, be discontinuous at these points. On the other hand, the trajectory of the muscle spike does *not* show a corner on $\dot{V}$ at the inflection points. Either the muscle fiber in contrast to the axon has a continuous membrane current, or the discontinuities shown by Rosenblueth, *et al.* were unintentionally introduced into the axon spike when a smoothed tracing was made from the original record. However, the portion of the response under question is about $10 - 30$ μsec. in duration and presumably during this time interval the membrane is changing from its resting to its "active" state. This is a decidedly short fraction of the total spike response and difficulties are to be expected if a close graphical analysis is made of this region in a conventional record.

APPENDIX

The present application requires the recording of a signal V, the spike potential, against its first time derivative dV/dt. V is immediately available at the output of the preamplifier and is applied directly to the horizontal amplifier of the oscilloscope, Fig. 1. By some means (discussed below), a signal which is proportional to dV/dt must be obtained

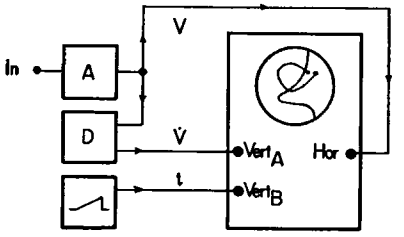

FIGURE 1 Schematic arrangement of preamplifier (A), differentiator (D), time base (t), and oscilloscope for simultaneous recording in (V, t) and (V, $\dot{V}$) coordinates. The oscilloscope horizontal and vertical amplifier inputs are appropriately indicated.

simultaneously for presentation *via* the vertical amplifier of the oscilloscope. If a dual-beam instrument is available, the second beam may be driven vertically by a saw-tooth time base t. This latter beam will plot the response in conventional coordinates, and is a useful adjunct to the phase trajectory (see Text Fig. 2).

There are several technical considerations affecting phase plane recording. These include (1) differentiation, (2) maintenance of the time relationship between the variables V and dV/dt, and (3) calibration.

Differentiators. One technique for electronic differentiation is based on the fact that capacitative current i_c is proportional to the first time derivative of the applied potential, $i_c = C\ dV/dt$. Since it is awkward to display current as such, various methods for converting i_c into a voltage signal have been developed; two are shown in Fig. 2.

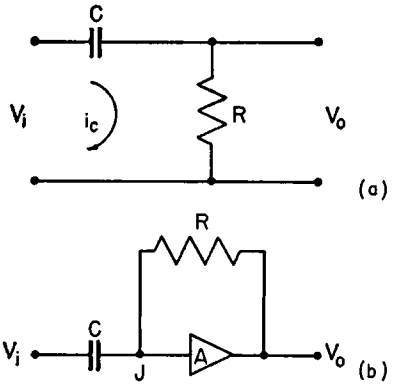

FIGURE 2(a) A passive differentiating network operating on V_i. Provided the time constant ($R \times C$) is small in comparison to the frequency of V_i, V_o will be directly proportional to dV_i/dt. However, certain errors are introduced as described in the text.

FIGURE 2(b) Operational amplifier (A) performing differentiation on V_i. For all practical purposes, the capacitance current $i_c = C\ (dV_i/dt)$ flowing into the junction point J is converted into a voltage $V_o = R \times i_c$. Thus $V_o = RC\ dV_i/dt$.

In a, (a high-pass filter used well below cutoff frequency), $V_o = i_c R = RC\ dV/dt$. Unfortunately, the voltage across the capacitor is altered from V_i to $(V_i - V_o)$ by R and the differentiation process is affected. For example, if a sine wave signal, $V_i = A \sin(\omega t)$, is applied to this network,

$$V_o = RCA \cdot \frac{1}{\sqrt{1 + \omega^2 R^2 C^2}} \cos(\omega t + \phi)$$

where $\phi = \arctan(-\omega RC)$. This is in marked contrast to the desired operation,

$$V_0 = RCA \cos(\omega t).$$

Two errors are thus introduced by the inclusion of the resistor. (1) The *amplitude* of the output signal is altered by the factor $1/\sqrt{1 + \omega^2 R^2 C^2}$. (2) The *time* relationship between V_i and V_o is modified by phase error ϕ, and the desired simultaneous registra-

tion of V and the dV/dt at the oscilloscope is perturbed. These errors are reducible by the selection of an RC product that is small in comparison to $1/\omega$. If $RC = 0.1/\omega$, the amplitude error is reduced to less than ½ per cent. On the other hand, the phase error ϕ is 5.7° or 0.1 radians. A 1 KCS signal will be delayed by $(0.1/2\pi)$ msec. or $\sim$ 16 μsec. While a time delay of this magnitude is rarely resolved in ordinary recording situations it does modify the phase plane trajectory by causing a clockwise rotation about the recording axes through an angle approximately equal to ϕ. Since these errors are frequency dependent, any complex biological signal is thereby variably compressed by amplitude error, and variably rotated by phase error. Although it is true that the amplitude and phase error may be further reduced by choosing $RC \ll 1/\omega$, this entails a decrease in gain and in the signal to noise ratio.

Fortunately, these errors are minimized by the active network shown in Fig. 2*b* which places an operational amplifier A across R. (A and R thus serve as a current-to-voltage converter operating on the capacitative current i_c.) The output voltage closely approaches $V_c = i_cR$ or $V_0 = -RC\ dV/dt$, and the amplitude and phase error of the passive network (a) are reduced by a factor $\sim 1/A$, where A is the open-circuit gain of the amplifier. A minimal cost amplifier designed for operation from a Tektronix 160-A power supply, is illustrated in Fig. 3. Its open-circuit gain, $\sim$80 to 100, will give satisfactory per-

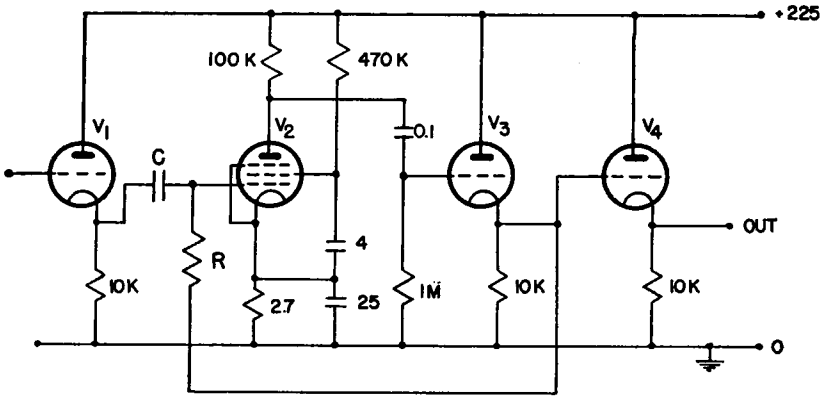

FIGURE 3 Practical design of the circuit shown in Fig. 2(b). V_1 and V_4 are required for decoupling the operational amplifier V_2 and V_3, from the preamplifier and the oscilloscope. This circuit operates from a Tektronix 160A power supply. V_1, V_3, V_4 are 12 AU7 tubes. V_2 is a 6267. All values for capacitors are in μf. The differentiating network C, R must be chosen according to the signal frequency. Cathode resistor of V_2 is 2700 ohms.

formance in most applications. The marked advantages offered by the active network permit an increase of RC to $1/\omega$ with subsequent improvement in the S/N ratio.

The present studies on the muscle spike were conducted with $RC = 1$ msec. Notice was taken of the reactance of the capacitor at signal frequency since this determined the input impedance of the differentiator. In addition, mica capacitors were chosen for C since these have high leakage resistance and show minimal soaking or absorption effects.

Time Delays. The filters and stray capacitances which limit the bandwidth of an amplifier introduce in all signals a frequency-dependent time delay, corresponding approximately to the phase error ϕ discussed above.

If f_{lo}, the low frequency cutoff of an amplifier is controlled by a single stage *RC* filter, the output leads the input. For any impressed frequency f,

$$\text{lead} = \frac{1}{2\pi f} \arctan\left(\frac{f_{lo}}{f}\right);$$

$$\text{lead} \simeq \frac{f_{lo}}{2\pi f^2} \qquad (\text{for } f \geq 10 f_{lo}).$$

On the other hand, a high frequency filter introduces a *lag* in the output signal,

$$\text{lag} = \frac{1}{2\pi f} \arctan\left(\frac{f}{f_{hi}}\right) \tag{1.1}$$

$$\text{lag} \simeq \frac{1}{2\pi f_{hi}}, \qquad (\text{for } f \leq 0.1 f_{hi}), \tag{1.2}$$

where f_{hi} is the upper cutoff frequency. Combining and rearranging gives the frequency-dependent delay of an *AC* amplifier,

$$\text{delay} = \frac{1}{2\pi f} \arctan\left\{\frac{f^2 - f_{lo} f_{hi}}{f(f_{lo} + f_{hi})}\right\}. \tag{2.1}$$

A positive value for delay implies a signal lag, while a negative value implies signal lead. Table I compares delays calculated from 2.1, for amplifiers of various bandwidths. The

TABLE I APPENDIX

SIGNAL DELAYS FOR INDICATED FREQUENCIES

Amplifier pass-band*	Signal frequency			
	10 cps	100 cps	1 kcs	10 kcs
10 c to 10 kc	−12.5 msec.	−144 μsec.	+14 μsec.	+12.5 μsec.
0 c to 300 kc	+0.5 μsec.	+0.5 μsec.	+0.5 μsec.	+0.5 μsec.
2 c to 300 kc	−3.2 msec.	−32 μsec.	+0.2 μsec.	+0.5 μsec.

* Response down by 3 db at the frequency limits indicated.

lead in a low frequency signal induced by the narrow band amplifier may be as much as 12½ per cent (!), while the signal delay inserted by the *DC* amplifier is dependent only on its upper cutoff frequency. The last entry was included to demonstrate the pronounced effect of the inclusion of low frequency filter in the wideband amplifier. The delays in Table I refer to single frequency components, and will degrade any complex waveform unless the amplifier has an adequate bandwidth. Note that these delays are usually small enough to be ignored in most V, t recording applications. However, the requirements in phase plane recording are more stringent. Prior to the appearance of the V signal at the input of the differentiator, the small phase errors introduced by the microelectrode and the preamplifier filters must be accepted. Thereafter, the time relationship between V and dV/dt must be preserved within a few microseconds, otherwise the resultant trajectory is rotated and compressed. This effectively demands wide-band amplification in the V and dV/dt signals once differentiation has occurred.

Calibration. The sine wave produced by a high quality generator, (such as the Ballantine 402 or the Hewlett Packard 206 A) is used for calibration of dV/dt signals. The waveform is generated as a voltage V, whose magnitude is

$$V = V_{max} \sin \omega t.$$

After differentiation, this sine wave is transformed to a voltage which is $V_d = RC\omega V_{max} \cos \omega t$. When V and V_d are led to the appropriate inputs of the oscilloscope, the sine wive is displayed in the phase plane as an ellipse, as shown elsewhere. Since ($\sin \omega t$) and ($\cos \omega t$) oscillate between $+1$ and -1, the peak to peak dV/dt deflection is thus equal to $2\omega RC\ V_{max}$, in volts/sec. The standard calibrating signal employed here is a 1 KCS, 100 mv $p - p$ sine wave. The V diameter of the resulting ellipse thus represents 100 mv, and is adjusted to cover five graticule units for convenience. The dV/dt diameter of the ellipse represents a first time derivative of 628 v/sec. (*i.e.*, 2×6280 sec.$^{-1} \times 50$ mv). This deflection is adjusted to span 6.3 graticule units.

When the calibrating signals are adjusted against the graticule as specified, a dV/dt axis deflection of 5 cm represents a derivative of 500 mv/msec., while a V axis deflection of 5 cm represents a voltage of 100 mv. This facilitates the measurement of any trajectory slope, which is $d(dV/dt)/dV$. In the present case, a 45° slope indicates a rate constant of (500 mv/msec.)/(100 mv) or 5 msec.$^{-1}$. Since tan 45° = 1, the slope of any linear trajectory in the phase plane multiplied by the scale factor 5 msec.$^{-1}$ gives the rate constant of the original exponential process. (It will be recalled that all signals which are exponential in time are transformed into linear trajectories.)

This particular calibration signal has another useful feature. Any phase error unintentionally introduced by the differentiator through an incorrect choice for the RC network or by unmatched amplification in the equipment will be immediately revealed through a rotation of the ellipse against the oscilloscope graticule. A rotation of 3 to 5° is apparent to the eye.

Other Practical Considerations. The beam blanking circuit of most oscilloscopes is ordinarily inactivated during $X - Y$ recording. This must be corrected, otherwise the beam is switched on continuously and may burn a hole in the phosphor or may over-expose camera film when the trajectory is at a nodal point (where V and dV/dt are simultaneously equal to zero as at the resting potential). (It is usually possible to rewire the blanking circuit so that the duration of beam brightening is controlled by the front panel switch for sweep speed and responds to external trigger pulses. Any selected portion of a trajectory may thus be recorded.)

This paper is publication No. 550 from the Division of Basic Health Sciences.
The work was supported by grants (B-861, B-3272) from the National Institute of Neurological Diseases and Blindness.

Received for publication, January 19, 1963.

REFERENCES

COLE, K. S., ANTOSIEWICZ, H. A., and RABINOWITZ, P., 1955, Automatic computation of nerve excitation. *J. Soc. Ind. and Appl. Math.*, **3**, 153.

GRAHAM, D., and MCRUER, D., 1961, Analysis of Non-Linear Control Systems, New York, John Wiley & Sons, Inc.

JENERICK, H., 1957, The effects of calcium on several electrical properties of muscle membrane, *in* Proceedings of the First National Biophysics Conference, New Haven, Yale University Press, 377.

JENERICK, H., 1961, Ionic currents in membrane of active muscle fiber, *Nature*, **191**, 1074.
MINORSKY, N., 1947, Introduction to Non-Linear Mechanics, Ann Arbor, J. W. Edwards.
ROSENBLUETH, A., WIENER, N., PITTS, W., and GARCIA RAMOS, J., 1948, An account of the spike potential of axons, *J. Cell. and Comp. Physiol.*, **32**, 275.
SCHMITT, O. H., 1955, Dynamic negative admittance components in statically stable membranes, *in* Electrochemistry in Biology and Medicine (T. Shedlovsky, editor), New York, John Wiley & Sons, Inc., 91.
TASAKI, I., and HAGIWARA, S., 1957, Capacity of muscle membrane, *Am. J. Physiol.*, **188**, 423.